Structure, Vol. 8, 1267–1278, December, 2000, ©2000 Elsevier Science Ltd. All rights reserved. PII S0969-2126(00)00536-0

A Cluster Exposed: Structure of the Rieske Ferredoxin from Biphenyl Dioxygenase and the Redox Properties of Rieske Fe-S Proteins

Christopher L. Colbert,* Manon M.-J. Couture,† Lindsay D. Eltis,†‡‖ and Jeffrey T. Bolin*§
*Department of Biological Sciences
Purdue University
West Lafayette, Indiana 47907
†Department of Microbiology and Immunology
University of British Columbia
Vancouver, British Columbia V6T 1Z3
Canada and
‡Department of Biochemistry
Pavillon Marchand
Université Laval
Québec City, Québec G1K 7P4
Canada

Summary

Background: Ring-hydroxylating dioxygenases are multicomponent systems that initiate biodegradation of aromatic compounds. Many dioxygenase systems include Rieske-type ferredoxins with amino acid sequences and redox properties remarkably different from the Rieske proteins of proton-translocating respiratory and photosynthetic complexes. In the latter, the $[Fe_2S_2]$ clusters lie near the protein surface, operate at potentials above +300 mV at pH 7, and express pH- and ionic strength–dependent redox behavior. The reduction potentials of the dioxygenase ferredoxins are approximately −150 mV and are pH-independent. These distinctions were predicted to arise from differences in the exposure of the cluster and/or interactions of the histidine ligands.

Results: The crystal structure of BphF, the Rieske-type ferredoxin associated with biphenyl dioxygenase, was determined by multiwavelength anomalous diffraction and refined at 1.6 Å resolution. The structure of BphF was compared with other Rieske proteins at several levels. BphF has the same two-domain fold as other Rieske proteins, but it lacks all insertions that give the others unique structural features. The BphF Fe-S cluster and its histidine ligands are exposed. However, the cluster has a significantly different environment in that five fewer polar groups interact strongly with the cluster sulfide or the cysteinyl ligands.

Conclusions: BphF has structural features consistent with a minimal and perhaps archetypical Rieske protein. Variations in redox potentials among Rieske clusters appear to be largely the result of local electrostatic interactions with protein partial charges. Moreover, it appears that the redox-linked ionizations of the Rieske proteins from proton-translocating complexes are also promoted by these electrostatic interactions.

§To whom correspondence should be addressed (e-mail: jtb@cc.purdue.edu).
‖Current address: Department of Microbiology and Immunology, University of British Columbia, Vancouver, British Columbia V6T 1Z3, Canada.

Introduction

Proteins containing Fe-S centers are essential for a variety of primary biological functions, such as respiration, photosynthesis, and enzymatic transformations [1]. The Fe-S clusters are generally redox active, and Fe-S proteins exploit nearly the full range of biologically relevant reduction potentials by modulating the Fe^{III}/Fe^{II} couple [2]. These proteins are widely distributed, and it has been suggested that simple Fe-S proteins may have been primordial proteins [3-5]. Thus, studies of the means by which Fe-S proteins control redox properties and affect electron transfer are of general significance.

In a typical protein bound Fe-S cluster, Fe atoms are bound to four sulfur atoms in a tetrahedral geometry [6]. In the rubredoxins, for example, a single Fe atom is bound by four cysteinyl thiolates. The various standard ferredoxins (including the HiPIPs according to current nomenclature [7]) possess $[Fe_2S_2(Cys)_4]$, $[Fe_3S_4(Cys)_3]$, or $[Fe_4S_4(Cys_4)]$ centers wherein the Fe atoms are bound to the protein by cysteinyl residues and are linked to each other by μ−sulfido (S^{2-}) bridges.

Variations on these well-known forms include the construction of larger metallocofactors by elaboration or fusion of the basic units as well as the use of non-cysteinyl protein ligands [5, 6]. Rieske-type Fe-S proteins provide a notable example of the latter. Spectroscopic studies of several Rieske proteins (reviewed in [8, 9]) and subsequent analysis of crystal structures [10, 11] established the presence of the $[Fe_2S_2]$ core, with one Fe bound by two cysteines and the second by two histidines. Both Fe atoms are ferric in the oxidized center, so that the core is $[Fe_2S_2]^{2+}$ and the cluster-ligand complex is $[(Cys)_2Fe^{III}(\mu_2\text{-}S)_2Fe^{III}(His)_2]^0$. The spectroscopic properties of the histidine-ligated Fe change upon reduction so that the reduced Rieske center is formally $[Fe_2S_2]^{1+}$, or $[(Cys)_2Fe^{III}(\mu_2\text{-}S)_2Fe^{II}(His)_2]^{1-}$. Standard 2Fe ferredoxins exploit the same core oxidation levels. However, the difference in the net charges of the ligands has a profound effect on the midpoint reduction potential; E_m values for standard 2Fe ferredoxins range from −450 to −250 mV (versus standard hydrogen electrode), whereas the values for Rieske-type proteins range from −160 to +360 mV.

For Rieske-type proteins, the wide range of reduction potentials reflects the existence of proteins in two classes that are distinguished by function as well as several redox properties. The first class is exemplified by membrane-associated Rieske proteins [12] that serve in eukaryotes and prokaryotes as components of respiratory or photosynthetic complexes. These proteins share two notable redox properties [9]; the E_m values are +265 to +320 mV near neutral pH, and the E_m titrates rapidly to lower values as pH is increased ($-\Delta E_m/pH > 60$ mV). Redox-linked ionization is potentially very significant because these proteins are components of proton-translocating complexes [13]. Two primary examples are associated with the mitochondrial cytochrome bc_1 complex and the cytochrome b_6f complex from chloroplasts. Rieske proteins from both complexes have been purified, characterized, and crystallized as soluble C-terminal fragments of approximately 130 residues. The fragments were prepared by proteolytic removal of N-ter-

Key words: biphenyl dioxygenase; Fe-S proteins; redox properties; Rieske ferredoxins

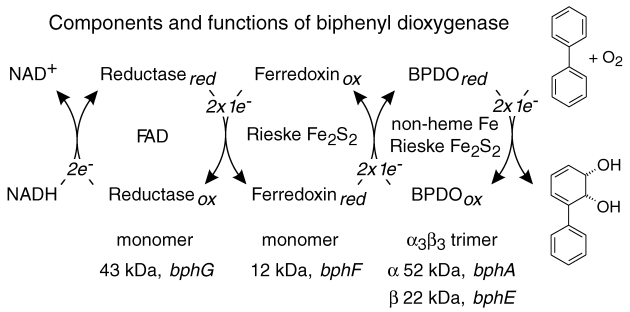

Figure 1. Components and Functions of the Biphenyl Dioxygenase System

The proposed electron transfer reactions and the conversion of biphenyl to *cis*-(2*R*,3*S*)-dihydroxy-1-phenylcyclohexa-4,6-diene [67] are illustrated. The abbreviation BPDO (biphenyl dioxygenase) identifies the catalytic component. Fundamental molecular properties of the proteins as well as the names of the associated genes (in italics) are listed at the bottom. The figure is adapted from [19].

minal membrane-tethering segments [14–16]. Crystal structures of such fragments from the bovine bc_1 [10] and spinach b_6f [11] complexes, known hereafter as bc1R and b6fR, were analyzed at 1.5 and 1.8 Å resolution, respectively. The structures are very similar in the vicinity of the cluster, which is located near the surface of the protein so that the histidine ligands are solvent exposed.

The second class includes soluble Rieske-type ferredoxins associated with multicomponent ring-hydroxylating dioxygenase systems, which catalyze a key step in the aerobic degradation of many aromatic compounds. The ferredoxins have approximately 110 residues and participate in pathways that deliver electrons from NAD(P)H to a mononuclear non-heme Fe^{II} active site located in the terminal component [17], as illustrated for biphenyl dioxygenase in Figure 1. Two well-characterized examples are BedB [18] and BphF [19] (M. M.-J. C. et al., submitted), which are associated with the benzene and biphenyl dioxygenases, respectively. BedB and BphF have 58% sequence identity with each other and 15%-20% pairwise identity with bc1R and b6fR. The redox properties of BphF and BedB are significantly different from those of proteins in the first class; the E_m values are around −150 mV near neutral pH, and they do not titrate. Moreover, the E_m of BedB was shown to be insensitive to ionic strength, whereas the E_m of bc1R was highly sensitive [18].

The terminal dioxygenase components also bind Rieske-type clusters with redox potentials similar to those of the ferredoxins [9, 17]. A recent crystal structure of naphthalene dioxygenase, NDO, showed that the cluster is bound by a 121 residue module of its α subunit (residues 38–158) that has a fold very similar to the higher-potential Rieske proteins [20]. NDO is an $\alpha_3\beta_3$ hexamer, and its three Rieske clusters are buried at interfaces between α subunits. NDOR will designate the Rieske module, which has 15%-20% sequence identity with bc1R, b6fR, BphF, and BedB.

Studies of other Fe-S and Cu-S proteins suggest that a variety of factors contribute to differences in redox potential between proteins with the same metal center and ligands [2, 21]. Key factors include the location of the metal center relative to electrostatic charges on protein atoms/groups, the polarizability of the atoms/groups, and the interactions of the metal center and protein with the solvent. Rigorous evaluation of these contributions requires a painstaking theoretical approach [22]. However, biochemical data and the coordinates provided by a crystal structure allow a first-level assessment of a metal center's location relative to partially or fully charged protein groups and the solvent boundary. Thus, comparison of the properties of BedB and bc1R [18] and determination of the structure of bc1R [10] supported a prediction that the Rieske clusters in BedB and other dioxygenase-linked ferredoxins should be buried within the protein and inaccessible to solvent [18]. Similarly, it was predicted that the histidine ligands in the ferredoxins were buried and/or involved in hydrogen bonds so that they could not titrate.

As part of our studies of biphenyl dioxygenase [23] and other enzymes involved in the biodegradation of PCBs [24–27], we determined the crystal structure of the associated ferredoxin, BphF, from *Burkholderia* sp. strain LB400. In this paper we analyze this structure, which, as far as we are aware, is the first available for a dioxygenase-linked Rieske ferredoxin. We also compare BphF to other proteins/domains that bind Rieske clusters, and we provide a detailed evaluation of structural features responsible for the distinctive redox properties of the two major classes of Rieske-type Fe-S proteins.

Results and Discussion

Structure Determination and Properties of the Model

We obtained an electron density map of high quality at a resolution of 2.5 Å via multiwavelength anomalous diffraction (MAD) phasing by exploiting the anomalous scattering of the intrinsic Fe atoms, as described in the Experimental Procedures. Refinement of the atomic model was completed at 1.6 Å resolution with $R = 18\%$ and $R_{free} = 20\%$. Figure 2 illustrates the quality of initial and final electron density maps, whereas Table 1 documents the content and quality of the final model.

The asymmetric unit contains two copies of BphF, molecules A and B. As indicated in Table 1, the final model includes residues 1–109 of both protein molecules as well as 313 water and 3 glycerol molecules. Ten side chain atoms from 4 residues are included at zero occupancy, whereas 84 atoms in 20 residues are modeled in multiple conformations. Superposition of all Cα atoms for A and B yielded a root-mean-square deviation (rmsd) of 0.61 Å, but this result is biased by poor superposition in four segments affected by crystal contacts or the presence of residues in alternate conformations. By excluding residues 1–5, 22–25, 53, 54, 95, and 96, the rmsd was reduced to 0.20 Å for 96 Cα atoms. Molecule B is the reference molecule for the discussion that follows because its model includes slightly fewer atoms in poor density or multiple conformations.

Both molecules include one residue, Asp-95, with (ϕ, ψ) torsion angles outside the allowed regions defined by PROCHECK [29]. Asp-95 is in a turn, has (ϕ, ψ) values near (+65°, −115°), and is represented by excellent density. The distribution and variation of *B* factors are reasonable except for two atoms in the alternate conformation of molecule A. The backbone O of residue 53 and the Cα of 54 are assigned occupancies of 0.5 but lie at positions that are probably occupied by water molecules in the primary conformation. These water molecules were not modeled for technical reasons. Thus, the scattering is underestimated, and the *B* factors are anomalously low.

The General Fold of BphF and Other Rieske Proteins

BphF demonstrates a fold consistent with those of bc1R, b6fR, and NDOR. Figure 3 shows that the fold is dominated by β structure and may be described as a stack of three β sheets

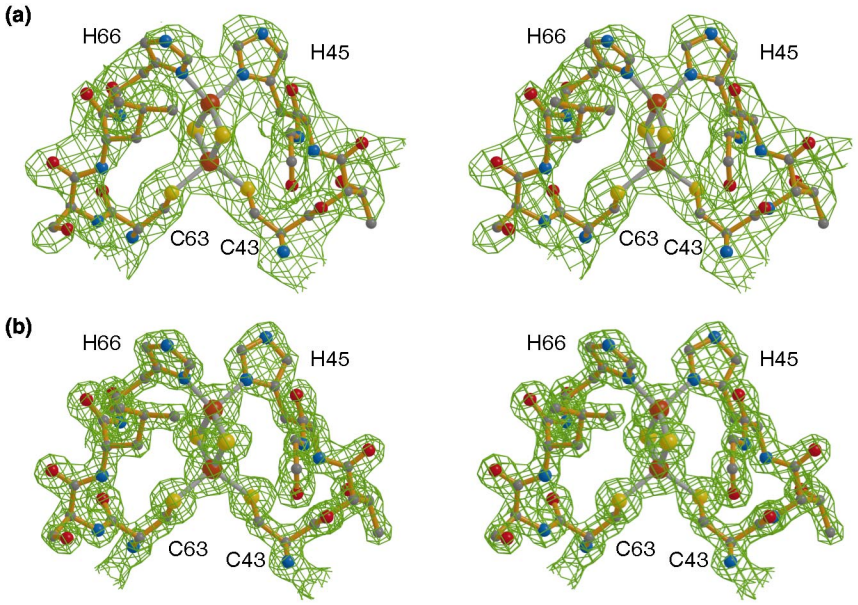

Figure 2. Electron Density Maps and Models Demonstrating the Quality and Resolution of the Initial and Refined Phases

Panels (a) and (b) are stereoscopic drawings. A portion of the refined model near the [Fe_2S_2] cluster in molecule B is illustrated in both panels. The $|F_o|$ electron density map in (a) was calculated at a resolution of 2.5 Å. MAD phases from a scattering model that included four Fe atoms in the asymmetric unit were used. It was contoured at 1σ, where σ is the standard deviation of a map with an average value of 0 e·Å^{-3}. Phases from the refined model were used to calculate the $2|F_o|-|F_c|$ map in (b) to a resolution of 1.6 Å, and the map was contoured at 2σ.

[10] or subdivided into two domains [11]. The cluster binding domain, or CBD, spans approximately 45 contiguous residues near the middle of the sequence and includes sheet 3 in the convention defined for bc1R [10]. Most of the residues N- or C-terminal to the CBD belong to a second, basal domain, or BD. This domain includes sheet 1, which is at the bottom in Figure 3, and sheet 2, near the middle. Figure 4 provides a structure-based sequence alignment developed from separate superpositions of CBDs and BDs. Global superpositions are unsatisfactory because the relative orientations of the two domains vary among the four proteins.

Table 1. Refinement Parameters and Statistics

Model Content (Non-Hydrogen Atoms)	
Protein atoms[a]	1,674
Fe(III) and S^{2-} atoms	8
Water oxygen atoms	313
Glycerol atoms	18
Diffraction Data	
Resolution range (Å)	26–1.6
Number of reflections[b]	33,172
$R_{refined}$ (%)	18.0
R_{free} (%)	20.0
Average *B* Values (Å^2)	
Protein atoms (backbone, side chain)	14.3, 18.2
Fe(III) and S^{2-} atoms	10.6
water oxygen atoms	31.3
glycerol atoms	20.5
all atoms	18.5
Rmsd from Restraints	
Bond lengths (Å)	0.011
Bond angles (°)	2.0
ΔB between bonded atoms (Å^2)	2.1

[a] The model includes residues 1–109 for each monomer, with 84 atoms in two conformations.
[b] The number of reflections used in the refinement. A total of 1761 distinct reflections contribute to R_{free}.

Similarities and Variations among the Cluster Binding Domains

For this discussion, we define the CBDs as the following segments: BphF, 41–86; bc1R, 137–180; b6fR, 105–147; and NDOR, 79–135 (including a unique 12 residue insertion). Superposing the BphF CBD with the others confirmed strong conservation of the fold at the level of the Cα trace [11] despite the fact that only the four cluster ligands and three additional residues are identical. In all cases, at least 37 Cα atoms can be superposed with an rmsd of less than 1.2 Å (see Table S1). The common structure begins with a β hairpin (BphF: 41–50), which is followed and opposed by an antiparallel β sheet, sheet 3 (BphF: 53–79). The sheet includes four strands except in NDOR, which lacks the first strand. The consensus CBD fold is completed by a proline-rich loop, called the Pro-loop (BphF: 80–86), that leads to the middle strand of sheet 1. NDOR again differs, as described below.

The initial hairpin and sheet 3 interact to form the core of the CBD, create two walls of the cluster binding site, and provide the ligands to the Fe-S cluster. A segment of approximately nine residues between the hairpin and the second strand of sheet 3 is conformationally variable within crystals of BphF as well as among the CBDs of the four different proteins. Thus, bc1R and b6fR superpose over the full CBD, except in the turn between the first two strands, but do not superpose with either of the two conformations in the BphF model until the start of the second strand. NDOR has distinctive structure prior to the second strand in that the backbone loops away from the CBD to interact with NDO's β subunits as well as the BD [20]. In consequence, NDOR lacks the initial strand of sheet 3 but superposes with the other CBDs over the final three strands.

In bc1R, b6fR, and BphF, the Pro-loop provides the third and final wall of the cluster binding site before it returns to the BD. NDOR has a 12 residue insertion at this site, and the chain extends away from the cluster to interact with an adjacent α subunit before returning to the common path just prior to rejoining the BD. A single tryptophan side chain (Trp-106) from sheet 3 establishes the third wall of the binding site in NDOR [20].

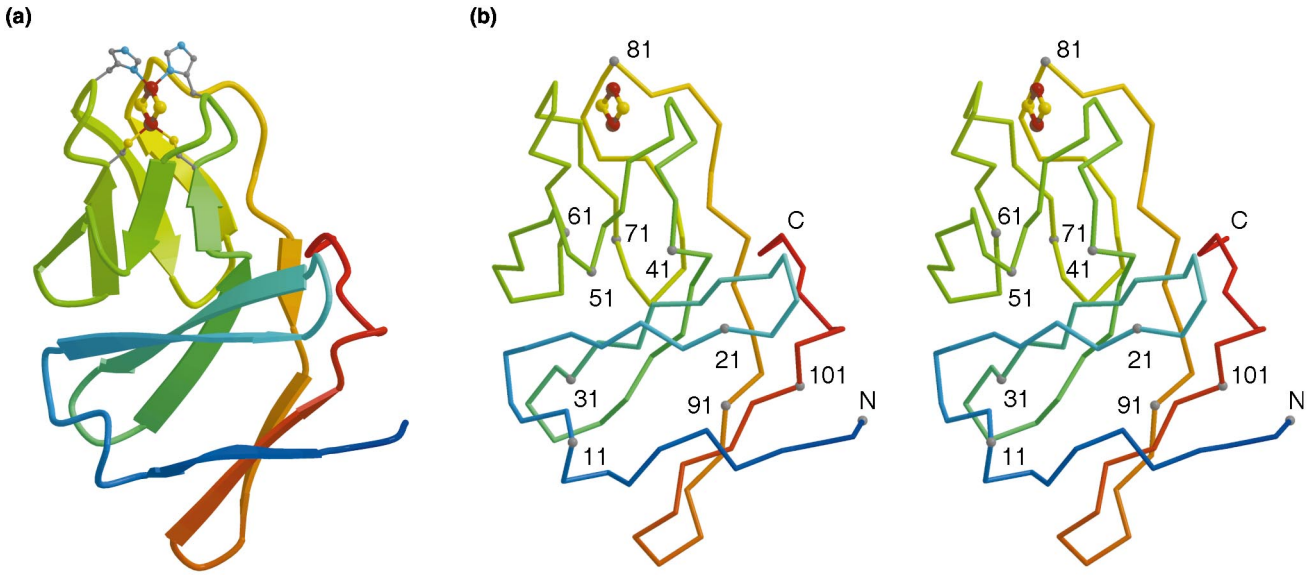

Figure 3. The Fold of BphF as Represented by the Course of the Backbone

Panel (a) is a ribbon drawing with β structure represented by arrows. Panel (b) is a stereoscopic Cα trace. Both panels are color ramped from blue at the N-terminus to red at the C-terminus. The [Fe_2S_2] cluster is plotted as a ball-and-stick rhombus, with Fe and S atoms colored red-brown and yellow, respectively. The ligands to the cluster are shown in (a), and every tenth Cα atom is plotted as a gray ball and numbered in (b).

Similarities and Variations among the Basal Domains

Although the four BDs include only one strictly conserved residue, the Cα traces are largely superposable, albeit with greater deviations than for the CBDs. The BD of BphF is most similar to that of NDOR, as quantified in Table S1 (see Supplementary Material). Both structures include a sandwiched pair of 3 strand, antiparallel β sheets, and there are no insertions/deletions larger than 1 residue. The first strand of sheet 1, β1, includes residues near the N terminus (BphF: 4–8), whereas the other two strands involve residues near the C terminus (BphF: 90–94 and 96–01). β1 is connected to sheet 2 by an irregular helical linker (BphF: 9–15). Sheet 2 spans approximately 25 residues (BphF: 16–40), and its final strand merges into the CBD. Sheets 1 and 2 are tacked together by hydrogen bonds between the final residues of sheet 2 and residues at the start of the middle strand of sheet 1 (strand β9.1 in Figure 4).

bc1R's BD has a similar core structure, but 26 additional residues inserted between strands β3 and β4 form a helix and a loop that extend along the CBD and interact extensively with it. The interactions vary in different crystalline forms of the bc_1 complex, and the variations appear to be functionally significant [30].

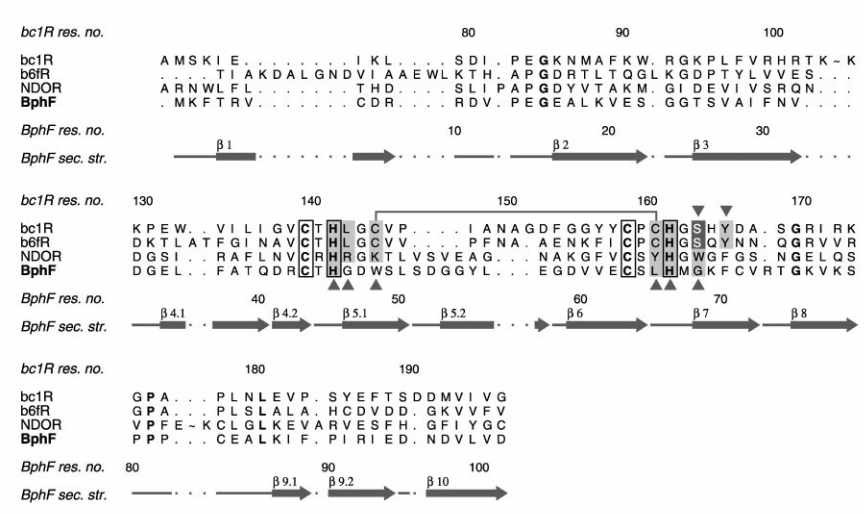

Figure 4. A Structure-Based Alignment of the Amino Acid Sequences of Four Rieske Proteins/Domains of Known Structure

The labels "bc1R", "b6fR", and "NDOR" indicate the sequences for the Rieske proteins or domains from the bovine mitochondrial cytochrome bc_1 complex, the spinach chloroplastic b_6f complex, and the α subunit of naphthalene dioxygenase from *Pseudomonas putida*. BphF is the Rieske-type ferredoxin of the biphenyl dioxygenase system from *Burkholderia* sp. strain LB400. Sequence numbers are plotted for bc1R (above) and BphF (below), and the secondary structure of BphF is plotted and labeled. The ligands of the [Fe_2S_2] cluster are boxed, and conserved residues are emboldened. Residues that form hydrogen bonds with the cluster sulfides or cysteinyl ligands are shaded and marked with triangles above and/or below if the hydrogen bond involves a side chain atom and/or a backbone amide, respectively. The sequences for all proteins are incomplete because of N- or C-terminal truncations or the elimination of large unique insertions, which are marked by the tilde symbol. All sequences were obtained from the Entrez server at the National Center for Biotechnology Information (USA). The accession numbers are 1942961, 2914267, 4699753, and P37322, in the order listed above. Atomic coordinates were acquired from PDB entries 1RIE (bc1R), 1RFS (b6fR), 1NDO (NDOR), and 1FQT (BphF).

BphF's BD is least similar to that of b6fR, which is the most structurally divergent domain. Part of the difference is associated with nonsuperposable C-terminal segments of differing length; b6fR is longer than BphF and bc1R by 9 and 16 residues, respectively. Additional structural divergence is traceable to insertions at three sites in the N-terminal part of b6fR (see Figure 4). One site is within strand β4, which is disrupted in b6fR by the addition of two residues. A second site occurs between strands β1 and β2. Whereas the other three structures possess a loosely helical connector, b6fR has a 4 residue insertion and a true 2 turn helix. The third site is a 7 residue insertion that maps to the middle of β1 and forms a β hairpin that loops out from β1 as a perturbation of the similar β structures observed in the other proteins. Moreover, this hairpin interacts through backbone hydrogen bonds with strand β2 (sheet 2) such that the fold of the BD in b6fR has been described as a barrel rather than a 2 sheet sandwich [11]. It is interesting that the latter two sites occur on the same face of b6fR, which may indicate a role in the interaction of b6fR with other proteins of the b_6f complex or with plastocyanin. A similar speculation can be applied to the lengthened C-terminal segment.

BphF as the Minimal Rieske Domain

In view of the above, BphF might be considered a minimal Rieske domain in the sense that it lacks each of the significant insertions or terminal extensions uniquely expressed in the other domains. Thus, BphF lacks the major insertion found in bc1R between β3 and β4. This insertion has been implicated in bc1R's apparent role as an anchored but mobile electron carrier. BphF also lacks the major insertion found in NDOR at the position of the Pro-loop. This insertion mediates the association of NDOR with a neighboring subunit as required for electron transfer to the non-heme Fe in the neighbor's active site. Finally, BphF lacks the insertions and C-terminal extension that distinguish the BD of b6fR. Should the additions in b6fR prove to have the proposed functional significance, then the concept of BphF as a minimal, and perhaps archetypical, Rieske-type protein would be firmly established; the minimal fold would have been augmented in each of the other domains to support electron transfer in a specific context. In the case of BphF, it is possible that the requirements of association and electron transfer with two unrelated protein partners has restricted augmentation of the core structure; it may be difficult to introduce significant changes that are compatible or advantageous with respect to both redox partners.

General Location of the Fe-S Cluster

The Fe-S cluster is located at the apex of the CBD with its two histidinyl ligands exposed to solvent, just as in the higher-potential bc_1 and b_6f Rieske fragments (see Figure 3). Placement near the surface of the protein fits a pattern common to the majority of small Fe-S proteins [21]. Although it is conceivable that the formation of oligomers in solution could sequester the cluster from the solvent, the crystal structure does not include contacts consistent with this concept. Although the clusters of both molecules A and B are occluded by similar dimeric, crystal-packing contacts, these contacts are associated with crystallographic 2_1 screw operations, which generate "infinite" chains of molecules rather than oligomers that might exist in solution. In addition, as illustrated in Figure 5b, these contacts are highly hydrated, as is typical of crystal contacts that are not expected to occur in solution [31].

The Environment of Rieske Fe-S Clusters: BphF Versus bc1R and b6fR

As illustrated in Figures 4 and 6, the cluster is bound between opposing β turns. Atom Fe1 is bound closer to the center of the CBD by Sγ atoms of two cysteines, 43 and 63, whereas Fe2 is bound closer to the surface by Nδ1 atoms of two histidines, 45 and 66. The cysteine and histidine ligands are paired, with the cysteine ligand in the strand leading into the turn and the histidine ligand within the turn. This arrangement is found in the structures of all four Rieske domains. Moreover, in consideration of the small rms differences between the atomic positions (0.14–0.17 Å) and variations in refinement procedures, the geometry of the eight cluster and ligand atoms is identical to within experimental error. However, in comparison to the higher-potential Rieske domains, structural variations in BphF remove both polar side chain and backbone amide groups from the vicinity of the cluster.

Relative to bc1R and b6fR, significant variations in sequence occur at and near BphF residues Trp-48, Leu-65, Gly-68, and Phe-70, which correspond to bc1R residues Cys-144, Cys-160, Ser-163, and Tyr-165. These residues are highlighted for BphF versus bc1R in Figure 6a; a comparison with b6fR would be equivalent. Differences in the interactions of the clusters and cysteine ligands with adjacent polar groups are illustrated in Figure 6b and documented in Table S2 (see Supplementary Material), which provides metric data for the key interactions in all four structures. As discussed below, these changes in the immediate vicinity of the cluster appear to be sufficient to lower the midpoint potential by the observed difference of approximately 500 mV through alteration of the electrostatic environment.

At the positions of BphF residues Gly-68 and Phe-70, interactions between cluster/ligand S atoms and polar side chains found in both bc1R and b6fR have been eliminated in BphF. The higher-potential proteins possess strictly conserved serine and tyrosine residues at these sites, and the serine Oγ and tyrosine Oη are within hydrogen bonding distance of the cluster sulfide atoms S1 and Sγ, respectively, of the first cysteinyl ligand. BphF and its homologs have residues incapable of forming side chain hydrogen bonds at both sites, glycine or alanine at position 68 and phenylalanine at position 70.

Changes in sequence at and near positions 48 and 65 affect interactions of the cluster with peptide dipoles. Whereas BphF and its homologs have nonpolar residues at positions 48 (tryptophan or alanine) and 65 (leucine), the higher-potential proteins possess strictly conserved cysteines that link the two cluster binding loops through a disulfide bond. The first of these cysteines occurs three residues after the initial histidine ligand, and the other occurs one position before the final histidine ligand. Differences in the flanking residues are associated with the presence or absence of the disulfide. It appears that the most significant changes precede the first cysteine, where a His-Leu-Gly-Cys sequence conserved in the higher-potential proteins [11] is replaced by His-Gly-Asp-Trp (residues 45-48) in BphF. The consequence is a dramatic reorientation of three consecutive peptides that removes two amide protons at positions 46 and 48 from the vicinity of the cluster sulfide atom S2 and rotates the positive pole of the peptide dipoles away from the cluster. Relative to bc1R, the calculated proton positions shift by 1.6 and 2.7 Å, the N-H-S angles change by 85° and 65°, and two NH-S hydrogen bonds implied by the structures of bc1R and b6fR are not possible. Instead, the displaced amide of Gly-46 associates with the carbonyl of Cys-43, and

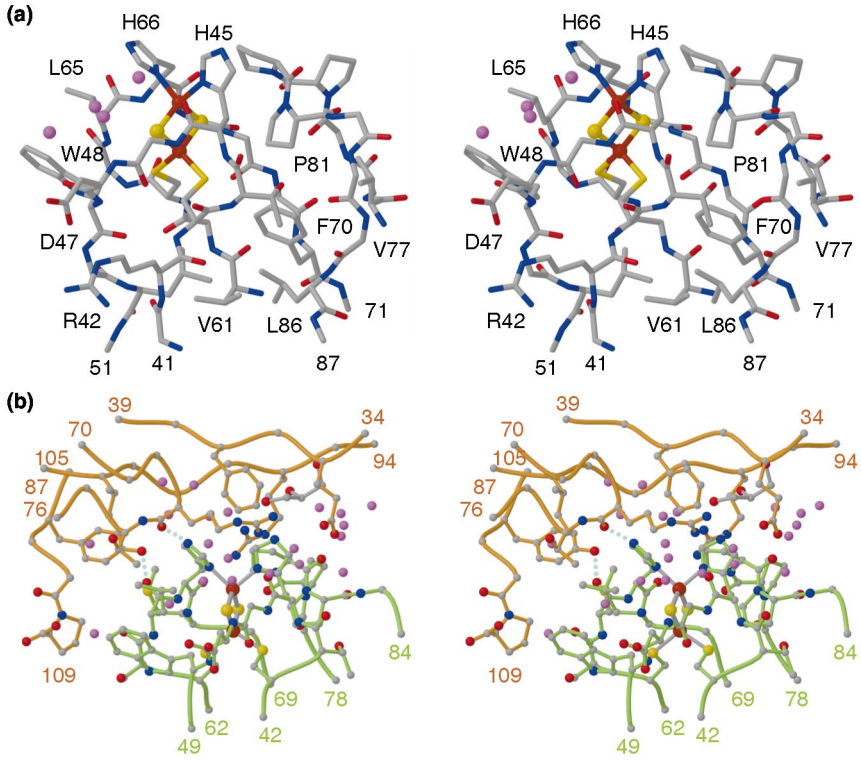

Figure 5. Stereoscopic Illustrations of the Environment of the Rieske Fe-S Center in the BphF Monomer and in the Crystal

Panel (a) illustrates the cluster binding domain in monomer B. Some side chains directed away from the Fe-S cluster were truncated to improve the visibility of features nearer to the cluster. C, N, O, S, and Fe atoms are colored gray, blue, red, yellow, and red-brown, respectively. Four water molecules are plotted as violet balls. Panel (b) illustrates the environment of the cluster in the crystal. The course of portions of the backbone for two molecules related by a 2_1 screw axis are plotted in green and gold, respectively. The colors of protein and water atoms are the same as in (a). Two intermolecular hydrogen bonds are represented by dotted lines.

the amide of Trp-48 forms a hydrogen bond with the carbonyl of Gly-46.

The positions and conformational freedom of the glycine residues are probably key factors in both variations, as is suggested for other Fe-S proteins [32]. In the structures of the higher-potential proteins, the (ϕ, ψ) values for the leucine-glycine pair are approximately (−130°, 10°) and (90°, 10°), and in BphF the values for the corresponding glycine–aspartic acid pair are (178°, 165°) and (−80°, 82°). Note that the (ϕ, ψ) values at glycine favor that amino acid over others in both cases. Moreover, the available sequences show strict conservation of glycine among the higher-potential proteins at the residue before the disulfide [11] and a strong preference (23 of 26 sequences) among BphF and its homologs for glycine one position closer to the N terminus.

On the opposing side of the cluster binding site, the presence or absence of the disulfide affects the interaction between a cluster sulfide atom and the backbone amide of the immediately following histidine ligand (BphF: 66). Although the amide has the proper orientation for hydrogen bonding with sulfide S1 in all structures, the nitrogen-to-sulfur and proton-to-sulfur distances are 0.7–0.8 Å longer in BphF than in bc1R or b6fR.

Three additional amide interactions are common to all of the structures and are relatively consistent in their metric parameters, as documented in Table S2. These interactions involve the amides of BphF residues His-45 with Sγ of the first cysteine ligand (Cys-43), Leu-65 with Sγ of the second cysteine ligand (Cys-63), and Gly-68 with sulfide S1.

Influence of Protein Structure on the Redox Potential: BphF Versus bc1R and b6fR

Figures 6c and 6d demonstrate that the calculated electrostatic potentials generated by the proteins at the surface of the Fe-S clusters (see Experimental Procedures) are significantly different for bc1R and BphF. At the positions of atoms Fe1, Fe2, S1, and S2, the calculated potentials are +34, +22, +33, and +27 *kT/q* for bc1R compared to +15, +9, +17, and +8 *kT/q* for BphF; the potentials for b6fR differ from bc1R by less than 2 *kT/q* at each atom. At 300 K, the differences between bc1R and BphF correspond to 475, 330, 420, and 505 mV at Fe1, Fe2, S1, and S2, respectively and thus are consistent with the difference in measured redox potentials. Although these results do not arise from rigorous calculations, the distribution of differences suggests not only that the cluster in BphF is less capable of accepting an electron at the redox-active Fe2 but also that the environment is less capable of assisting the delocalization of electron density from Fe2 to the other atoms.

Compared to bc1R and b6fR, the structure of BphF eliminates or significantly reduces the influence of five side chain and backbone interactions capable of stabilizing the reduced Rieske cluster. Importantly, four changes affect groups in contact with the cluster sulfides in the higher-potential proteins. Are these differences in local protein cluster interactions sufficient to change the reduction potential by approximately 500 mV? Although detailed theoretical and experimental studies will be required to fully address this question, an analysis of experimental results from related systems suggests that they could account for most if not all of the difference.

Site-directed mutagenesis of the higher-potential Rieske proteins from *Saccharomyces cerevisiae* [33] and *Paracoccus denitrificans* [34] recently allowed experimental tests of the influence of the two hydrogen bonding side chains on the reduction potential. Whereas the wild-type *Saccharomyces* protein had a potential of +285 mV at pH 7, a serine→alanine mutation lowered the potential by 130 mV to +155 mV, and a tyrosine→phenylalanine mutation lowered the potential to +217 mV; the potential for the double mutant was +105 mV.

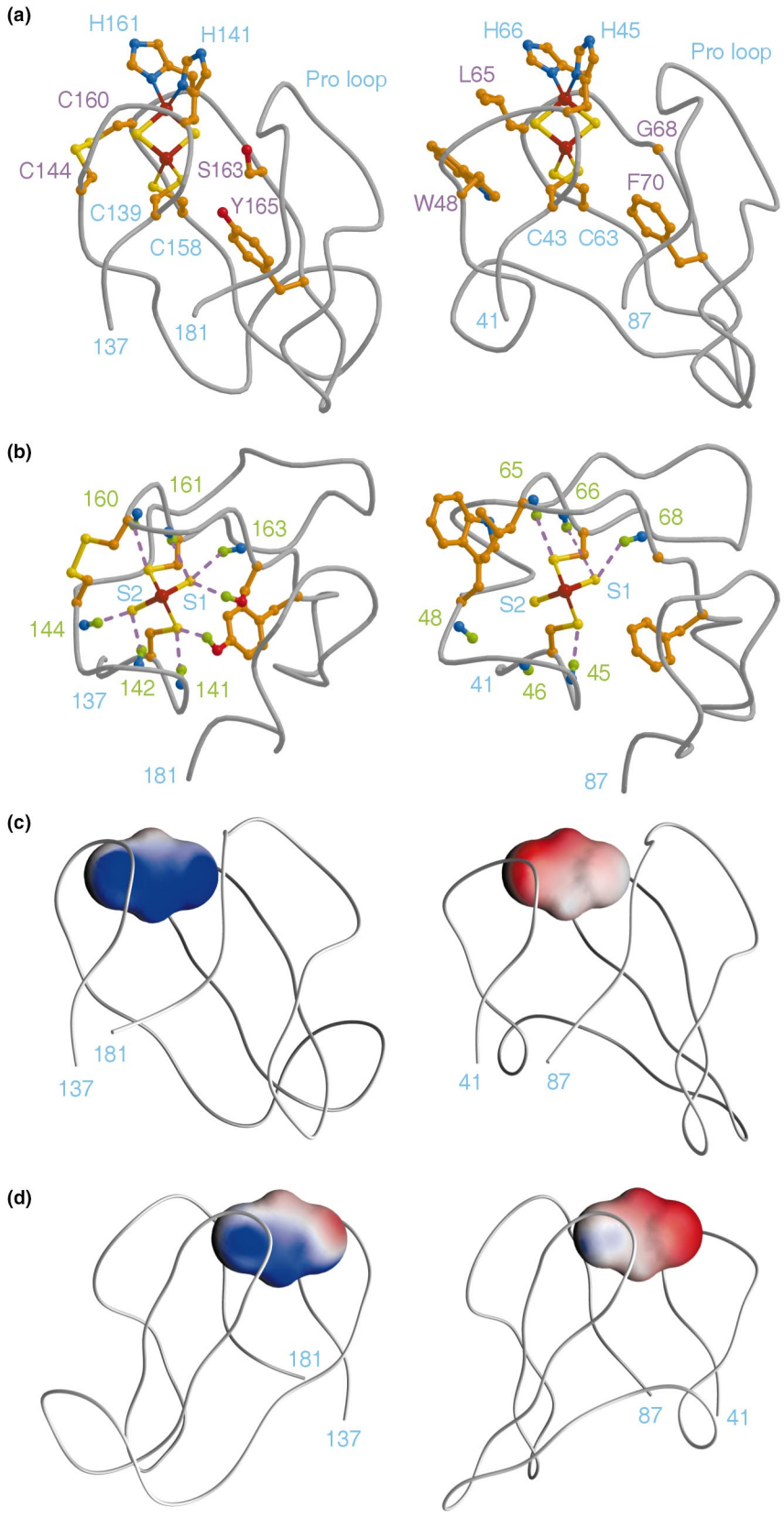

Figure 6. A Comparison of Key Structural Features and Electrostatic Potential Maps for bc1R and BphF

bc1R is shown on the left, and BphF is shown on the right. Panel (a) illustrates the course of the backbone in the cluster binding domain as well as key residues discussed in the text. Ligands and termini are labeled in blue, and variant residues are labeled in magenta. Fe2 is nearer to the top. In (b) the molecules have been rotated 90° about a horizontal axis, and the histidine ligands have been removed to reveal the interactions of polar groups with the cluster and ligand S atoms. Calculated H atoms are plotted as green spheres bonded to backbone N atoms (blue) or side chain O atoms (red). The residue numbers of the polar groups are plotted in green. The cluster sulfides S1 and S2 and the ligands are labeled in blue. Dashed red lines indicate potential hydrogen bonds to S atoms. Panels (c) and (d) illustrate electrostatic potential maps calculated at the molecular surface of the Fe-S cluster as described in the text. The view in (c) is rotated slightly from (a) about a vertical axis, and (d) is rotated 180° about the same axis from (c). The potential maps are plotted such that saturated red, white, and saturated blue correspond to 0, +20, and +40 *kT/q*, respectively. For bc1R, the extreme values on the surface are +8 and +87 *kT/q*; for BphF, they are −1 and +35 *kT/q*.

For the *Paracoccus* protein, the serine→alanine and tyrosine→phenylalanine mutants reduced the potential from +360 mV to +265 mV and +316 mV, respectively. It was suggested that the serine→alanine mutation generated a larger shift because the serine side chain interacts with the cluster sulfide, which is directly coupled to the redox-active iron [34].

Consideration of the influence of interactions between peptide groups and Fe-S clusters dates to the earliest comparisons of the structures of *Chromatium vinosum* HiPIP and the *Peptococcus aerogenes* ferredoxin [32, 35], both of which bind $[Fe_4S_4]$ clusters. The central hypothesis suggested that a greater number of NH-S hydrogen bonds enabled the ferredoxins to stabilize the cluster at the $[Fe_4S_4]^{2+:1+}$ couple at potentials below −200 mV, whereas the HiPIPs, with a smaller number, were restricted to the $[Fe_4S_4]^{3+:2+}$ couple at potentials above +100 mV. Although subsequent comparisons showed that the redox potentials of HiPIPs with the same number of NH-S interactions can vary by more than 200 mV [21], it remains clear that variations in peptide interactions can and do influence the reduction potential of Fe-S proteins. In one recent example, mutation of the *C. vinosum* HiPIP removed one amide proton from the vicinity of the cluster and lowered the E_m by 104 mV [36]. Other data pertinent to the $[Fe_4S_4]$ proteins are reviewed in [21].

Recent studies of rubredoxin variants demonstrate that sequence changes adjacent to conserved glycines can alter the interaction of a single peptide dipole and significantly change the reduction potential of an Fe-S protein. Thus, an analysis of sequences, structures, and calculated electrostatic potential predicted that a major cause of the difference between the potentials of the *Clostridium pasteurianum* (*Cp*) and *Pyrococcus furiosis* (*Pf*) rubredoxins arises from the identity of the residue Xaa in a Cys-Gly-Xaa sequence [37]. The cysteine is conserved as the last of the four ligands, and the conserved glycine residue has (ϕ, ψ) angles near (90°, 10°). This prediction was tested by evaluation of mutants where the identity of Xaa was exchanged in both systems [38]. For the wild-type *Pf* protein, Xaa = alanine, the midpoint potential was +37 mV, and the N-S distance is 3.5 Å (PDB entry 1CAA). For the wild-type *Cp* protein, Xaa = valine, the midpoint potential was −55 mV, and the distance from the backbone amide N to Sγ of the cysteine ligand was 3.8 Å (PDB entry 1IRO). The alanine→valine replacement in *Pf* lowered the potential to −58 mV, and the valine→alanine replacement in *Cp* raised the potential to +31 mV. In the crystal structure of the latter, the N-S distance decreased to 3.5 Å. Independent studies of the *Cp* protein confirmed the results obtained for the valine→alanine replacement [39]. Moreover, the critical role of glycine residues within the ligand binding loops has been similarly demonstrated by studies of several additional mutants [40, 41].

These are especially relevant examples because the mononuclear Fe atom in rubredoxins is bound by four cysteine residues located on β ladders resembling those of the Rieske proteins and situated at approximately the same distance from the protein-solvent boundary [10]. Based on these examples, it is clear that reorientation or displacement of three peptide dipoles in the immediate vicinity of the cluster, as seen when BphF is compared to bc1R, should make a major contribution to the total difference in redox potential.

The contributions of more remote, fully charged groups and of differences in the influence of the solvent are additional factors that might influence the redox potentials of the Rieske clusters. With respect to the former, calculations of electrostatic potential suggest that negatively charged, surface-exposed side chains in the vicinity of the BphF cluster may contribute to its lower redox potential, but not to a large extent. BphF has a calculated pI of 4.7, and there are five aspartic acid/glutamic acid side chains within 15 Å of the cluster (as measured by the distance from the aspartic acid Cγ or glutamic acid Cδ atoms to the closest cluster atom). BedB also has aspartic acid/glutamic acid residues at these sites and the same calculated pI, which is typical for dioxygenase ferredoxins. Truncation of the individual residues to alanine had a small effect on electrostatic potentials calculated at the positions of the cluster atoms; the maximum change at a single atom was +1 kT/q. The maximum change with all five residues truncated was +3.6 kT/q. It appears that the ensemble of acidic residues may contribute to the lowered potential but that no specific residue plays a major role.

Although the Rieske cluster is bound relatively near the surface, it is not expected that differences in solvent interactions with the cluster or protein make a dominant contribution to the differences in redox potentials. Comparisons of BphF to either bc1R or b6fR demonstrate that the general shapes of the proteins and locations of the clusters are remarkably similar and that the calculated solvent accessibilities of the cluster and ligand atoms vary insignificantly.

pH Dependence of the Redox Potentials of bc1R, b6fR, and Related Rieske Proteins

The E_m of BphF varies linearly as a function of pH over the pH range of 5.0–10.0, with a small $\Delta E_m/pH = -8$ mV/pH (M. M.-J.C. et al., submitted). BedB, which is 75% identical in sequence to BphF in the cluster binding domain, shows similar behavior [18]. In contrast, the reduction potentials of the oxidized forms of bc1R and b6fR show a marked decline with the functional form of a titration curve. In electrochemical studies of bc1R, ΔE_m ranged from −60 mV/pH near pH 7 to −120 mV/pH at pH 10, and the overall variation was fit by two titratable groups in the oxidized protein with $pK_{ox1} = 7.6$ and $pK_{ox2} = 9.2$ [14]. Optical titrations of b6fR in the pH range 5.0 to 8.0 indicated a similar ΔE_m/pH near pH 7 and an apparent pK of 6.5 [16]. Many other Rieske proteins from diverse organisms have E_m values above +100 mV at pH 7 and show redox-linked ionizations [42–48]. For some acidophiles, pK_{ox1} and pK_{ox2} values as low as 6.2 and 8.5 have been reported [45, 46, 48].

The common view has been to assign the pK near 8 to one of the histidinyl ligands [14, 46, 49]. The assignments of pH-dependent features in resonance Raman spectra from the *Thermus thermophilus* [49] and *Sulfolobus* [46] proteins to Fe-N stretching frequencies provide one line of supporting evidence. Furthermore, the Mössbauer parameters of the redox-active Fe in the *Thermus* protein, i.e., the Fe coordinated by the two histidinyl ligands, varied with pH [43]. Apart from the spectroscopic results, the established ability of metal centers to shift the pK values of ligands is also cited [49]. Thus, the normal pK of 14.2 for deprotonation of imidazole to imidazolate shifted to values in the range of 8.9–10 for cations of the type $[(NH_3)_5M(imH)]^{3+}$, where M = Cr^{III}, Co^{III}, or Ru^{III}, and imH = imidazole [50]. For the anionic complexes $[(CN)_5Fe^{III}(RimH)]^{2-}$, where R = H or CH_3, the measured pK was 10.4 [51].

The lower potential of BedB and the absence of pH or ionic-strength dependence have been attributed to significant differences in the environment of its cluster and/or histidine ligands. The proposals included burial of the cluster within the monomer, burial of the cluster within a dimer, and stabilization of the imidazole form of the histidine ligand by hydrogen bonding

[9, 18]. Based on the high sequence identity between the CBDs of BedB and BphF, their very similar circular dichroic spectra, and the shared property of a pH-independent E_m, these explanations should be equally applicable to BedB and BphF. However, the structure of BphF argues against all of these explanations. First, the cluster is not buried in the BphF monomer, and the dimeric contacts in the crystal structure are not consistent with formation of a solution phase dimer that would bury the cluster. Moreover, the electrochemical properties of BphF were established under conditions where the protein is monomeric (M. M.-J. C. et al., submitted). Second, the histidine ligands, especially the Nε2 atoms, are exposed to solvent, and neither Nε2 atom is within 9 Å of an acidic side chain that might stabilize the imidazole form.

We also considered whether some basic side chain other than the histidine ligands might play a key role in the redox-linked ionization of the higher-potential proteins. For example, the titration of a positively charged group proximal to the cluster could be responsible for the observed pH dependence [46]. Alternatively, if a histidine ligand is indeed the titrating group, the unusually large p*K*a shift could be promoted by interactions with a nontitrating side chain [43]. However, in the crystal structures of bc1R and b6fR, neither the histidine ligands nor the clusters are closely approached by a basic side chain. In bc1R, the closest base is Arg-118, which is 9.2 Å or more away from the histidine Nε2 positions or any cluster atom. The closest candidate in b6fR is Arg-140, which is at least 8.8 Å away.

Thus, the structural data for bc1R, b6fR, and BphF do not suggest a reasonable alternative to the proposal that a histidine ligand titrates from imidazole to imidazolate in the higher-potential proteins. Nevertheless, the structure of BphF clearly demonstrates that the environment of the histidine ligands is sufficiently similar in bc1R, b6fR, and BphF that differences in interactions of the histidines with solvent or nearby protein side chains are highly unlikely to be responsible for the presence or absence of redox-linked ionization. With respect to the full $[Fe_2S_2(Cys)_2(His)_2]$ system, deprotonation of an imidazole ligand of the oxidized system is similar to reduction of the cluster in that the overall charge of the system changes from 0 to −1. Perhaps the ensemble of structural features responsible for the large difference in redox potential is also responsible for the presence or absence of a redox-linked ionization near pH 8. In other words, relative to BphF and its homologs, the total environment of the oxidized cluster-ligand system in the higher-potential proteins apparently allows the system to more readily accept a full electronic charge, whether that charge arises from reduction of the metal or from deprotonation of a ligand. Thus the environment can either raise the reduction potential by 500 mV or lower the p*K* of a coordinated imidazole group by 6 log units.

The reduced and ligand-deprotonated states are formally different and should have different charge distributions. However, it is expected that an imidazolate ligand will donate electron density to the oxidized cluster [6, 51], which should both lower the reduction potential, as observed, and permit interactions between the cluster and protein to help stabilize the ionized ligand. Further studies of the electronic properties of the Rieske proteins, and especially the alkaline pH states of the higher-potential proteins, are clearly warranted. If a histidine ligand does indeed titrate to the imidazolate form, the p*K* shift is quite remarkable in that it significantly exceeds the shifts observed in model cationic-transition metal complexes [50], as reviewed above.

Table 2. Diffraction Measurements and Phasing Statistics

Energy (keV)	7.138	7.117	13.000
Wavelength (Å)	1.737	1.742	0.9537
Number observations	72,073	77,520	166,227
Number unique reflections	17,158	19,208	65,959
d_{min} (Å)	2.5	2.4	1.6
Redundancy	4.2	4.0	2.52
Completeness (%)	97.4	96.2	98.5
last shell[a]	95.6	86.5	97.2
R_{sym} (%)	5.3	5.2	6.0
Last shell	10.1	14.5	37.2
Phasing Statistics for Reflections in the Range of 20.0–2.5 Å			
R_{Cullis}[b]			
Dispersive, centric	0.61	0.47	—
Dispersive, acentric	0.49	0.40	—
Anomalous	0.71	0.77	—
Phasing Power[c]			
Centric	1.46	2.08	—
Acentric	2.73	3.63	—

Figures of Merit		
Centric	Acentric	All
0.74	0.78	0.78

[a] Last shells are 2.59–2.5 Å, 2.49–2.4 Å, and 1.66–1.6 Å for λ = 1.737 Å, 1.742 Å, and 0.9537 Å, respectively.

[b] R_{Cullis} for the dispersive data is the mean lack of closure divided by the mean dispersive difference, with 0.9537 Å used as the reference wavelength; for the anomalous data it is the mean lack of closure divided by the mean anomalous difference.

[c] Phasing power = mean $|F_A|$ divided by the mean lack of closure, where $|F_A|$ is the amplitude of the calculated structure factor of the anomalous scatterers.

Structure and Redox Potential: BphF Versus NDOR

The local environment of the Rieske cluster in NDOR shares some but not all of the differences that distinguish BphF from the higher-potential proteins. Like BphF, NDOR lacks the serine and tyrosine side chain interactions observed in bc1R and b6fR. However, in the segment that follows the first histidine ligand, the amide groups of NDOR residues Arg-84 and Lys-86 interact with sulfide S2, as seen in bc1R and b6fR but not in BphF (see Table S2). Note that the sequence in NDOR (residues 83–86) is His-Arg-Gly-Lys-, where Lys-86 corresponds to the first disulfide bonded cysteine in bc1R and b6fR. The importance of a glycine residue for formation of the amide interactions is again implied by (ϕ, ψ) values of (87°, 18°) at Gly-85. On the opposite side of the cluster binding site, the amide of ligand His-104 interacts with sulfide S2 as in the higher-potential proteins, not at the longer distance observed in BphF.

The reduction potential of the Rieske center in NDO has not been reported. On the basis of the above, it should be expected that the potential would be intermediate between those of BphF and bc1R. However, the potentials of the Rieske centers in benzene dioxygenase, −110 mV [52], and phthalate dioxygenase, −150 mV [53], are close to that of BphF. If the potential of the Rieske center in NDO similarly approaches that of BphF, factors distinct from those identified in the comparison of BphF and the higher-potential proteins are likely to be involved. For example, both histidine ligands in NDO are hydrogen bonded to side chain carboxylates from a neighboring α subunit, and it is reasonable to expect that these interactions influence the

reduction potential, as previously suggested [20]. Differences in solvent interactions are also more likely to be important because the cluster in NDOR is sequestered at a subunit interface.

Biological Implications

Rieske-type Fe-S proteins are critical components of electron transfer pathways at the core of fundamental biological processes such as respiration, photosynthesis, and the biodegradation of aromatic compounds. Electron transfers within such systems are controlled by the protein components, which modulate the properties of the metal centers. Remarkably different properties have been established for two important classes of Rieske Fe-S proteins. The analysis presented here clarifies the structural origins of these variations.

Rieske proteins from the bc_1 or b_6f complexes have redox potentials near +300 mV and demonstrate redox-linked ionizations that may be a critical feature of these proton-translocating complexes. In contrast, the Rieske-type ferredoxins from the dioxygenase systems set the redox potential near –150 mV and do not exhibit the ionization. Prior to this study, the working models suggested that these differences arose from variations in the location of the clusters relative to the protein-solvent boundary and/or differential interactions of the histidine ligands with other protein groups.

Determination of the structure of BphF, a dioxygenase-linked ferredoxin from the biphenyl/PCB catabolic pathway, establishes that the structure of the ferredoxins is very similar to that of the higher-potential proteins. Comparisons among the proteins suggest that BphF may represent the minimal and archetypical Rieske fold. The BphF structure also shows that its Rieske cluster is not buried, but rather is bound near the protein-solvent boundary, just as in the higher-potential proteins. The analysis predicts that differences in the immediate interactions of the clusters with a small number of nearby side chain and peptide polar groups establish both the redox potential and the presence or absence of redox-linked ionizations.

Experimental Procedures

Protein Source, Purification, and Crystallization

A thorough description of bacterial strains, plasmids, genetic manipulations, and procedures for protein purification and crystallization is provided elsewhere (M. M.-J. C. et al., submitted). In brief, the *bphf* gene from *Burkholderia* sp. strain LB400 [54, 55] was expressed from a plasmid in *Escherichia coli*. An N-terminal histidine tag was added to facilitate purification and was eventually removed to yield a recombinant protein extended by three residues, with an N-terminal sequence NH_3^+-Gly-Ser-His-Met[1]. The protein was purified, stored, and crystallized in the oxidized form under anaerobic conditions. Crystals were grown in a glove box (Innovative Technologies) under nitrogen atmosphere ($\leq$ 2 ppm O_2) at 10° C by the seeded, sitting-drop vapor diffusion method. Fresh seed stocks containing 25% PEG 4000, 50 mM $MgCl_2$, 100 mM Tris-HCl (pH 8.5), and 1 mM DTT were prepared by serial dilution of the supernatant from a centrifuged suspension of crystals that were mechanically crushed in the same buffer. In a typical crystallization, 1 μL of the seed solution and 2 μL of a reservoir solution containing 25% polyethylene glycol monomethyl ether 5000 (or PEG 4000), 0.2 M ammonium sulfate, and 0.1 M MES buffer (pH 6.5) was added to 3 μL of a protein solution containing 31 mg/mL rcBphF, 0.150 M sodium chloride, 1 mM DTT, and 20 mM MOPS buffer (pH 7.0). The crystals grow in clusters with a rod-like habit and dimensions of 0.05–0.15 mm in the smallest dimension and up to 2 mm in the longest. The crystals have the space group $P2_12_12$ with a = 76.3 Å, b = 52.6 Å, and c = 65.0 Å, and there are two molecules of BphF in the asymmetric unit.

Diffraction Measurements

To prepare crystals for all diffraction experiments, we added approximately 30 μL of well solution to the drop and incubated the crystals for approximately 1 hr prior to mounting them or exposing them to solutions containing cryoprotectants. For experiments at cryogenic temperatures, the crystals were incubated for 2–5 min in each of four solutions containing the well solution augmented by 5%, 10%, 15%, and 20% v/v glycerol. We flash froze the crystals within the glove box by plunging them into liquid nitrogen. The crystals were stored under liquid nitrogen until they were used in diffraction experiments.

Diffraction data from a single crystal were used for refinement as well as for initial phasing by the multiwavelength anomalous diffraction (MAD) method. The data were acquired by the use of beamline BM14D at the Advanced Photon Source (APS) at Argonne National Laboratory with the support of the BioCARS collaborative access team. Synchrotron radiation was rendered monochromatic (bandpass was approximately 1–2 eV) by a Si(111) double-crystal monochromator and focused by a toroidally-shaped, Rh-coated Si mirror. An inverse-beam strategy was used to measure diffraction images from one frozen crystal at four energies, in the order 13.000, 7.117, 7.138, and 8.041 keV. The nominal temperature of the gas stream was 100 K, and the energies are approximate because the monochromator was not calibrated during these experiments. X-ray fluorescence spectra recorded in the vicinity of the Fe-K absorption edge established that the middle of the rising edge occurred at the nominal energy of 7.117 keV. Diffraction images were recorded by a Quantum-1 CCD detector (Area Detector Systems Corporation, Poway, CA), and they were analyzed and reduced to scaled intensities with the HKL package [56]. The data acquired at the first three energies are summarized in Table 2; those measured at 8.041 keV were affected by systematic errors of unknown origin and were not used.

MAD Phasing and Phase Improvement

Programs from the CCP4 software package [57] were used for scaling between data sets, phase determination, and phase improvement. The MAD data were treated as if they were from isomorphous derivatives. Structure factor amplitudes from the two energies near 7.1 keV were scaled to the reference data acquired at 13 keV. The positions of the two $[Fe_2S_2]$ clusters were determined by analysis of an anomalous-difference Patterson map calculated with data in the resolution range of 10–3.5 Å. The program MLPHARE [58] was used within the CCP4 package to refine positional and scattering parameters for the clusters and to calculate initial phases. An electron density map based on data in the range of 20–3.5 Å revealed the approximate positions of the four individual Fe atoms. MLPHARE was again used to refine the parameters of a four-Fe scattering model and to calculate phases to 2.5 Å resolution. Statistics from the phase calculations are included in Table 2. Solvent flattening, as implemented in the CCP4 program DM, was then used to improve the phases before the first model was obtained by interpretation of a 2.5 Å resolution map.

Model Building and Refinement

O [59] was used to display electron density maps and to construct, revise, and analyze atomic models. CNS [60] was used with a maximum likelihood target function for automated refinement against the data acquired at 13 keV. An initial model was constructed with reference to maps at 2.5 Å resolution and refined by one round of restrained minimization of positional and grouped B factors. The resolution was extended to 1.6 Å, and two rounds of model building and restrained minimization, first with grouped B factors and then individual atomic B factors, produced a model with R = 28.3% and R_{free} = 30.6%. The model for the protein component was essentially correct at this stage. The addition of bound waters, glycerol molecules, and protein components in alternative conformations completed the refinement with R = 18.0% and R_{free} = 20.0%. Additional statistics are provided in Table 1. The geometry within the Fe-S cluster and the bonds with protein ligands were moderately restrained with the following force constants: 200 kcal·mole^{-1}·Å^{-2} applied to Fe-S (target = 2.28 Å), Fe-Nδ1 (2.05 Å), and Fe-Fe (2.68 Å) distances; and 40 kcal·mole^{-1}·rad^{-2} applied to angles S-Fe-Nδ1 (115°), S-Fe-S (105°), Fe-S-Fe (75°), Nδ1-Fe-Nδ1 (90°), Fe-Nδ1-Cγ (108°), and Fe-S-Cβ (109.5°).

Calculations of Electrostatic Potential and Preparation of Figures

Protons were added to crystal structures through the use of QUANTA (Molecular Simulations) or REDUCE [61]. DELPHI [62] was used to calculate electrostatic potentials on successively finer grids of 1.05, 0.53, 0.35, and

0.26 Å; at the final spacing the potential was calculated three times. The results were analyzed and displayed with GRASP [63]. As far as we could determine, accurate partial charges have not been established for Rieske clusters in any state. Therefore, rigorous calculations of electrostatic potential with the cluster included are not possible, and the calculations serve primarily to provide a graphical demonstration of the electrostatic influence of the remainder of the solvated protein at the cluster or its ligands. For this purpose, the partial charges on the Fe and S atoms of the cluster were set to zero, and the charges on the ligand atoms were altered to those of alanine. That is, the partial charges on Cβ, 1Hβ, and 2Hβ were set to the values for alanine, the partial charge of 3Hβ was assigned to the Cys-Sγ or His-Cγ atom, and all other atoms in the imidazole rings of histidine ligands were assigned zero partial charge. The programs MOLSCRIPT [64] and RASTER3D [65] were used to prepare Figures 4, 5, 6a, and 6b. Figure 2 was prepared with BOBSCRIPT [66] and RASTER3D. Figures 6c and 6d were prepared with GRASP.

Supplementary Material

Supplementary material including Tables S1 and S2 is available at http://current-biology.com/suppmat.supmatin.htm.

Acknowledgments

This research was supported in part by award GM-52381 from the National Institutes of Health (to J. T. B.) and by operating grant OGP0171359 from the Natural Sciences and Engineering Research Council of Canada (to L. D. E.). C. L. C. was supported in part by institutional training award GM-08296 from the National Institutes of Health. M. M.-J. C. is the recipient of a studentship from the FCAR of Québec, Canada. Use of the Advanced Photon Source was supported by the US Department of Energy, Basic Energy Sciences, Office of Energy Research, under Contract W-31-109-Eng-38. BioCARS Sector 14 was supported by the National Institutes of Health, National Center for Research Resources, through grant RR-07707. The assistance and efforts of the BioCARS staff are gratefully acknowledged.

Received: July 10, 2000
Revised: September 18, 2000
Accepted: October 3, 2000

References

1. Beinert, H., Holm, R.H., and Münck, E. (1997). Iron-sulfur clusters: nature's modular, multipurpose structures. Science *277*, 653–659.
2. Capozzi, F., Ciurli, S., and Luchinat, C. (1998). Coordination sphere versus protein environment as determinants of electronic and functional properties of iron-sulfur proteins. Struct. Bonding *90*, 127–160.
3. Hall, D.O., Cammack, R., and Rao, K.K. (1971). Role for ferredoxins in the origin of life and biological evolution. Nature *233*, 136–138.
4. Meyer, J. (1988). The evolution of ferredoxins. Trends Ecol. Evol. *3*, 222–226.
5. Beinert, H. (2000). Iron-sulfur proteins: ancient structures, still full of surprises. J. Biol. Inorg. Chem. *5*, 2–15.
6. Holm, R.H., Kennepohl, P., and Solomon, E.I. (1996). Structural and functional aspects of metal sites in biology. Chem. Rev. *96*, 2239–2314.
7. Nomenclature Committee of the International Union of Biochemistry (NC-IUB) (1991). Nomenclature of electron-transfer proteins: recommendations 1989. Eur. J. Biochem. *200*, 599–611.
8. Shergill, J.K., and Cammack, R. (1994). ESEEM and ENDOR studies of the Rieske iron-sulphur protein in bovine heart mitochondrial membranes. Biochim. Biophys. Acta *1185*, 35–42.
9. Link, T.A. (1999). The structures of Rieske and Rieske-type proteins. Adv. Inorg. Chem. *47*, 83–157.
10. Iwata, S., Saynovits, M., Link, T.A., and Michel, H. (1996). Structure of a water soluble fragment of the "Rieske" iron-sulfur protein of the bovine heart mitochondrial cytochrome *bc*1 complex determined by MAD phasing at 1.5 Å resolution. Structure *4*, 567–579.
11. Carrell, C.J., Zhang, H., Cramer, W.A., and Smith, J.L. (1997). Biological identity and diversity in photosynthesis and respiration: structure of the lumen-side domain of the chloroplast Rieske protein. Structure *5*, 1613–1625.
12. Rieske, J.S., MacLennan, D.H., and Coleman, R. (1964). Isolation and properties of an iron-protein from the (reduced coenzyme Q)-cytochrome c reductase complex of the respiratory chain. Biochem. Biophys. Res. Commun. *15*, 338–344.
13. Link, T.A., and Iwata, S. (1996). Functional implications of the structure of the "Rieske" iron-sulfur protein of bovine heart mitochondrial cytochrome *bc*1 complex. Biochim. Biophys. Acta *1275*, 54–60.
14. Link, T.A., Hagen, W.R., Pierik, A.J., Assmann, C., and von Jagow, G. (1992). Determination of the redox properties of the Rieske [2Fe-2S] cluster of bovine heart *bc*1 complex by direct electrochemistry of a water-soluble fragment. Eur. J. Biochem. *208*, 685–691.
15. Link, T.A., Saynovits, M., Assmann, C., Iwata, S., Ohnishi, T., and von Jagow, G. (1996). Isolation, characterisation and crystallisation of a water-soluble fragment of the Rieske iron-sulfur protein of bovine heart mitochondrial *bc*1 complex. Eur. J. Biochem. *237*, 71–75.
16. Zhang, H., et al., and Cramer, W.A. (1996). Characterization and crystallization of the lumen side domain of the chloroplast Rieske iron-sulfur protein. J. Biol. Chem. *271*, 31360–31366.
17. Butler, C.S., and Mason, J.R. (1997). Structure-function analysis of the bacterial aromatic ring-hydroxylating dioxygenases. Adv. Microb. Physiol. *38*, 47–84.
18. Link, T.A., Hatzfeld, O.M., Unalkat, P., Shergill, J.K., Cammack, R., and Mason, J.R. (1996). Comparison of the "Rieske" [2Fe-2S] center in the *bc*1 complex and in bacterial dioxygenases by circular dichroism spectroscopy and cyclic voltammetry. Biochemistry *35*, 7546–7552.
19. Haddock, J.D., Pelletier, D.A., and Gibson, D.T. (1997). Purification and properties of ferredoxinBPH, a component of biphenyl 2,3-dioxygenase of *Pseudomonas* sp strain LB400. J. Ind. Microbiol. Biotechnol. *19*, 355–359.
20. Kauppi, B., et al., and Ramaswamy, S. (1998). Structure of an aromatic-ring-hydroxylating dioxygenase-naphthalene 1,2-dioxygenase. Structure *6*, 571–586.
21. Stephens, P.J., Jollie, D.R., and Warshel, A. (1996). Protein control of redox potentials of iron-sulfur proteins. Chem. Rev. *96*, 2491–2513.
22. Warshel, A., Papazyan, A., and Muegge, I. (1997). Microscopic and semimacroscopic redox calculations: what can and cannot be learned from continuum models. J. Biol. Inorg. Chem. *2*, 143–152.
23. Imbeault, N.Y.R., Powlowski, J.B., Colbert, C.L., Bolin, J.T., and Eltis, L.D. (2000). Steady-state kinetic characterization and crystallization of a polychlorinated biphenyl-transforming dioxygenase. J. Biol. Chem. *275*, 12430–12437.
24. Han, S., Eltis, L.D., Timmis, K.N., Muchmore, S.W., and Bolin, J.T. (1995). Crystal structure of the biphenyl-cleaving extradiol dioxygenase from a PCB-degrading pseudomonad. Science *270*, 976–980.
25. Vaillancourt, F.H., Han, S., Fortin, P.D., Bolin, J.T., and Eltis, L.D. (1998). Molecular basis for the stabilization and inhibition of 2,3-dihydroxybiphenyl 1,2-dioxygenase by *t*-butanol. J. Biol. Chem. *273*, 34887–34895.
26. Seah, S.Y., Terracina, G., Bolin, J.T., Riebel, P., Snieckus, V., and Eltis, L.D. (1998). Purification and preliminary characterization of a serine hydrolase involved in the microbial degradation of polychlorinated biphenyls. J. Biol. Chem. *273*, 22943–22949.
27. Seah, S.Y.K., Labbé, G., Nerdinger, S., Johnson, M.R., Snieckus, V., and Eltis, L.D. (2000). Identification of a serine hydrolase as a key determinant in the microbial degradation of polychlorinated biphenyls. J. Biol. Chem. *275*, 15701–15708.
28. Berman, H.M., et al., and Bourne, P.E. (2000). The Protein Data Bank. Nucleic Acids Research *28*, 235–242.
29. Laskowski, R., MacArthur, M.W., Moss, D.S., and Thornton, J.M. (1993). PROCHECK: a program to check the stereochemical quality of protein structures. J. Appl. Crystallogr. *26*, 283–291.
30. Iwata, S., et al., and Jap, B.K. (1998). Complete structure of the 11-subunit bovine mitochondrial cytochrome *bc*1 complex. Science *281*, 64–71.
31. Janin, J., and Rodier, F. (1995). Protein-protein interaction at crystal contacts. Proteins *23*, 580–587.
32. Adman, E., Watenpaugh, K.D., and Jensen, L.H. (1975). NH···S hydrogen bonds in *Peptococcus aerogenes* ferredoxin, *Clostridium pasteurianum* rubredoxin, and *Chromatium* high potential iron protein. Proc. Natl. Acad. Sci. USA. *72*, 4854–4858.
33. Denke, E., Merbitz-Zahradnik, T., Hatzfeld, O.M., Snyder, C.H., Link, T.A., and Trumpower, B.L. (1998). Alteration of the midpoint potential and catalytic activity of the Rieske iron-sulfur protein by changes of amino acids forming hydrogen bonds to the iron-sulfur cluster. J. Biol. Chem. *273*, 9085–9093.
34. Schröter, T., et al., and Link, T.A. (1998). Mutational analysis of residues forming hydrogen bonds in the Rieske [2Fe-2S] cluster of the cyto-

chrome *bc*1 complex in *Paracoccus denitrificans*. Eur. J. Biochem. *255*, 100–106.
35. Carter, C.W., Jr., Kraut, J., Freer, S.T., and Alden, R.A. (1974). Comparison of oxidation-reduction site geometries in oxidized and reduced *Chromatium* high potential iron protein and oxidized *Peptococcus aerogenes* ferredoxin. J. Biol. Chem. *249*, 6339–6346.
36. Babini, E., Borsari, M., Capozzi, F., Eltis, L.D., and Luchinat, C. (1999). Experimental evidence for the role of buried polar groups in determining the reduction potential of metalloproteins: the S79P variant of *Chromatium vinosum* HiPIP. J. Biol. Inorg. Chem. *4*, 692–700.
37. Swartz, P.D., Beck, B.W., and Ichiye, T. (1996). Structural origins of redox potentials in Fe-S proteins: electrostatic potentials of crystal structures. Biophys. J. *71*, 2958–2969.
38. Eidsness, M.K., et al., and Kang, C. (1999). Modulation of the redox potential of the [Fe(SCys)4] site in rubredoxin by the orientation of a peptide dipole. Biochemistry *38*, 14803–14809.
39. Xiao, Z.G., Maher, M.J., Cross, M., Bond, C.S., Guss, J.M., and Wedd, A.G. (2000). Mutation of the surface valine residues 8 and 44 in the rubredoxin from *Clostridium pasteurianum*: solvent access versus structural changes as determinants of reversible potential. J. Biol. Inorg. Chem. *5*, 75–84.
40. Ayhan, M., et al., and Wedd, A.G. (1996). The rubredoxin from *Clostridium pasteurianum*: mutation of the conserved glycine residues 10 and 43 to alanine and valine. Inorg. Chem. *35*, 5902–5911.
41. Maher, M.J., Xiao, Z., Wilce, M.C., Guss, J.M., and Wedd, A.G. (1999). Rubredoxin from *Clostridium pasteurianum*. Structures of G10A, G43A and G10VG43A mutant proteins. Mutation of conserved glycine 10 to valine causes the 9-10 peptide link to invert. Acta Crystallogr. D Biol. Crystallogr. *55*, 962–968.
42. Prince, R.G., and Dutton, P.L. (1976). Further studies on the Rieske iron-sulfur center in mitochondrial and photosynthetic systems: a p*K* on the oxidized form. FEBS Lett. *65*, 117–119.
43. Kuila, D., and Fee, J.A. (1986). Evidence for a redox-linked ionizable group associated with the [2Fe-2S] cluster of *Thermus* Rieske protein. J. Biol. Chem. *261*, 2768–2771.
44. Liebl, U., Pezennec, S., Riedel, A., Kellner, E., and Nitschke, W. (1992). The Rieske FeS center from the Gram-positive bacterium PS3 and its interaction with the menaquinone pool studied by EPR. J. Biol. Chem. *267*, 14068–14072.
45. Anemüller, S., Schmidt, C.L., Schäfer, G., Bill, E., Trautwein, A.X., and Teixeira, M. (1994). Evidence for a two proton dependent redox equilibrium in an archaeal Rieske iron-sulfur cluster. Biochem. Biophys. Res. Commun. *202*, 252–257.
46. Iwasaki, T., Imai, T., Urushiyama, A., and Oshima, T. (1996). Redox-linked ionization of sulredoxin, an archaeal Rieske-type [2Fe-2S] protein from *Sulfolobus* sp. strain 7. J. Biol. Chem. *271*, 27659–27663.
47. Brugna, M., Albouy, D., and Nitschke, W. (1998). Diversity of cytochrome *bc* complexes: example of the Rieske protein in green sulfur bacteria. J. Bacteriol. *180*, 3719–3723.
48. Brugna, M., Nitschke, W., Asso, M., Guigliarelli, B., Lemesle-Meunier, D., and Schmidt, C. (1999). Redox components of cytochrome *bc*-type enzymes in acidophilic prokaryotes II: the Rieske protein of phylogenetically distant acidophilic organisms. J. Biol. Chem. *274*, 16766–16772.
49. Kuila, D., et al., and Woodruff, W.H. (1992). Resonance Raman studies of Rieske-type proteins. Biochim. Biophys. Acta *1140*, 175–183.
50. Winter, J.A., Caruso, D., and Shepherd, R.E. (1988). Influence of pentaamminechromium(III) on the acidity of coordinated imidazoles and pyrazole. Inorg. Chem. *27*, 1086–1089.
51. Johnson, C.R., Shepherd, R.E., Marr, B., O'Donnell, S., and Dressick, W. (1980). Affinities of imidazolate and imidazole ligands for pentacyanoiron(III). J. Am. Chem. Soc. *102*, 6227–6235.
52. Geary, P.J., Saboowalla, F., Patil, D., and Cammack, R. (1984). An investigation of the iron-sulphur proteins of benzene dioxygenase from *Pseudomonas putida* by electron-spin-resonance spectroscopy. Biochem. J. *217*, 667–673.
53. Gassner, G.T., Ludwig, M.L., Gatti, D.L., Correll, C.C., and Ballou, D.P. (1995). Structure and mechanism of the iron-sulfur flavoprotein phthalate dioxygenase reductase. FASEB J. *9*, 1411–1418.
54. Erickson, B.D., and Mondello, F.J. (1992). Nucleotide sequencing and transcriptional mapping of the genes encoding biphenyl dioxygenase, a multicomponent polychlorinated-biphenyl-degrading enzyme in *Pseudomonas* strain LB400. J. Bacteriol. *174*, 2903–2912.
55. Hofer, B., Eltis, L.D., Dowling, D.N., and Timmis, K.N. (1993). Genetic analysis of a *Pseudomonas* locus encoding a pathway for biphenyl/polychlorinated biphenyl degradation. Gene *130*, 47–55.
56. Otwinowski, Z., and Minor, W. (1997). Processing of X-ray diffraction data collected in oscillation mode. Methods Enzymol. *276*, 307–326.
57. Dodson, E.J., Winn, M., and Ralph, A. (1997). Collaborative computational project, number 4: providing programs for protein crystallography. Methods Enzymol. *277*, 620–633.
58. Otwinowski, Z. (1991). Maximum likelihood refinement of heavy atom parameters. In Isomorphous Replacement and Anomalous Scattering, W. Wolf, P.R.E., and A. G. W. Leslie, ed. (Daresbury, U. K: Science and Engineering Research Council Daresbury Laboratory), pp. 80–86.
59. Jones, T.A., Zou, J.Y., Cowan, S.W., and Kjeldgaard, M. (1991). Improved methods for building protein models in electron density maps and the location of errors in these models. Acta Crystallogr. A *47*, 110–119.
60. Brünger, A.T., et al., and Warren, G.L. (1998). Crystallography & NMR System: a new software suite for macromolecular structure determination. Acta Crystallogr. D Biol. Crystallogr. *54*, 905–921.
61. Word, J.M., Lovell, S.C., Richardson, J.S., and Richardson, D.C. (1999). Asparagine and glutamine: using hydrogen atom contacts in the choice of side-chain amide orientation. J. Mol. Biol. *285*, 1735–1747.
62. Nicholls, A., and Honig, B. (1991). A rapid finite difference algorithm, utilizing successive over-relaxation to solve the Poisson-Boltzmann equation. J. Comput. Chem. *12*, 435–445.
63. Nicholls, A., Sharp, K.A., and Honig, B. (1991). Protein folding and association: insights from the interfacial and thermodynamic properties of hydrocarbons. Proteins *11*, 281–296.
64. Kraulis, P.J. (1991). Molscript: a program to produce both detailed and schematic plots of protein structures. J. Appl. Crystallogr. *24*, 946–950.
65. Merritt, E.A., and Bacon, D.J. (1997). Raster3D: photorealistic molecular graphics. Methods Enzymol. *277*, 505–524.
66. Esnouf, R.M. (1997). An extensively modified version of MolScript that includes greatly enhanced coloring capabilities. J. Mol. Graph. Model. *15*, 132–134.
67. Gibson, D.T., Roberts, R.L., Wells, M.C., and Kobal, V.M. (1973). Oxidation of biphenyl by a *Beijerinckia* species. Biochem. Biophys. Res. Commun. *50*, 211–219.

Accession Numbers

The coordinates were deposited in the Protein Data Bank [28] as entry 1FQT.

Note Added in Proof

The paper cited in the text as "M. M.-J. C. et al., submitted" has been accepted for publication (M. M.-J. C., et al., and L. D. E. [2000]. Characterization of BphF, a Rieske-type ferredoxin with a low reduction potential. Biochemistry, in press).